Nonuniform corticothalamic continuum model of electroencephalographic spectra with application to split-alpha peaks

P. A. Robinson,[1,2,*] R. W. Whitehouse, and C. J. Rennie[1,2]
[1]*School of Physics, University of Sydney, New South Wales 2006, Australia*
[2]*Brain Dynamics Center, University of Sydney and Westmead Hospital, Westmead, New South Wales 2145, Australia*
(Received 26 July 2002; published 28 August 2003)

Recent theoretical work has successfully predicted electroencephalographic spectra from physiology using a model corticothalamic system with spatially uniform parameters. The present work incorporates parameter nonuniformities into this model via the coupling they induce between spatial eigenmodes. Splitting of the spectral alpha peak, an effect seen in a small percentage of the normal population, is investigated as an illustrative special case. It is confirmed that weak splitting can arise from mode structure if the peak is sufficiently sharp, even for uniform parameters. However, it is further demonstrated that greater splitting can result from nonuniformities, and it is argued that this mechanism for split alpha is better able to account quantitatively for this effect than previously suggested alternatives of pacemakers or purely cortical resonances. On introducing nonuniformities in corticothalamic loop time delays, we find that the alpha frequency also varies as one moves from the front to the back of the head, in accord with observations, and that analogous (but less distinct) variations are seen in the beta peak. Analysis shows realistic variations of around ± 10 ms relative to the mean loop delay of approximately 80 ms can account for observed splittings of about 1 Hz. It is also suggested that subjects who display clear alpha splitting form the tail of a distribution of magnitude of cortical inhomogeneity, rather than a separate population.

DOI: 10.1103/PhysRevE.68.021922 PACS number(s): 87.10.+e, 87.19.Nn, 87.19.La, 87.90.+y

I. INTRODUCTION

Electroencephalographic (EEG) measurements are commonly made using multiple scalp electrodes. Correlations of EEGs with brain function are widely used diagnostically [1,2], and are inferred to be closely connected to brain dynamics, information processing, cognition, and state of arousal [1–3]. EEGs result from cortical electrical activity aggregated over scales much larger than individual neurons. Hence, one approach to understanding their dynamics is via models that average over microscopic neural structure to obtain continuum descriptions on scales of millimeters to the whole brain, incorporating realistic anatomy such as separate excitatory and inhibitory neural populations (pyramidal cells and interneurons), nonlinear neural responses, multiscale interconnections, dendritic, cell-body, and axonal dynamics, and corticothalamic feedback [2,4–21].

A recent physiologically based continuum model of corticothalamic dynamics has been found to reproduce many features of normal EEGs, including the discrete spectral peaks in the slow wave (<1 Hz), delta (1–2.5 Hz), theta (2.5–7.5 Hz), alpha (7.5–12.5 Hz), and beta (12.5–30 Hz) bands, seen in waking and sleeping states [12,14–20]. Here we extend this model to include spatial nonuniformities of its parameters, an essential step since many or all of these are nonuniform in practice. This generalized model is then applied to understanding observed substructure in the alpha peak.

Splitting of the alpha peak into two subpeaks, separated by up to 1–2 Hz, has been found to occur in a small percentage of the normal population [19]. One mechanism that could account for such a splitting is that of pacemakers located in the thalamus or other parts of the brain, each of which comprises neurons with a characteristic frequency [1,2]. This mechanism then attributes each subpeak to a different pacemaker. Although neurons with resonant frequencies certainly exist, a severe problem with this theory is its *ad hoc* justification for why a particular resonant frequency is produced. Indeed, under this mechanism, a new pacemaker is needed for every peak or subpeak. Another problem is that the transition from waking to sleep would involve deactivation of waking peaks, with concurrent activation of others at intermediate frequencies, and this pattern is not explained by pacemaker theory [19]. A second widely discussed mechanism is that resonances may result from spatial cortical eigenmodes [2]. This mechanism implies that the frequencies of the global resonances should not depend on the location in the cortex, although their amplitudes may. In this picture, the splitting of the alpha peak is predicted to be due to breaking of an initial degeneracy between modes as a result of cortical asymmetry [2]. Since the posterior lobes of the brain are larger, smaller wave numbers k and frequencies ω should then be dominant in amplitude in this region, all else being equal [19]. Equivalently, the higher frequency mode of an initially degenerate pair should tend to have higher amplitudes in frontal regions [2], which is contrary to observation [19]. A third mechanism, suggested recently [19], is that the observed splitting may arise from nonuniformities of the time delay in corticothalamic loops whose resonances give rise to the spectral peaks. This suggestion is investigated below as a specific test and illustration of our generalized model.

In Sec. II we generalize our previous theory to include nonuniformities via coupling of spatial eigenmodes. In Sec.

*Electronic address: p.robinson@physics.usyd.edu.au

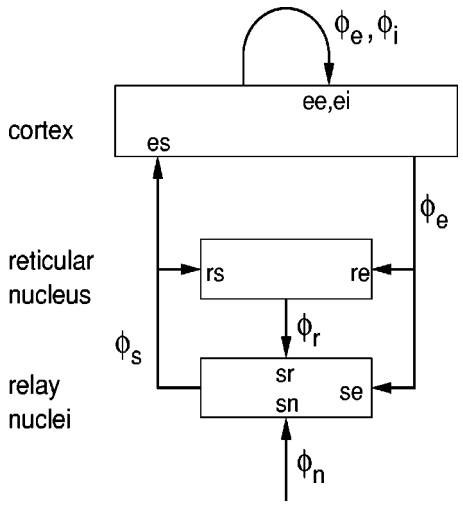

FIG. 1. Schematic of corticothalamic interactions, showing the connectivities and locations ab of the gains G_{ab} for impulses from neurons b incident on neurons of type a. The cortex and the reticular and relay nuclei of the thalamus are shown as rectangles, along with the main neural projections between them (the latter are indicated by arrows, labeled with the type of activity that projects). External activity is indicated by ϕ_n.

III we illustrate the method using the specific case of nonuniform corticothalamic time delay as applied to split-alpha spectra.

II. THEORY

In this section we briefly outline our uniform corticothalamic model, generalizing it to incorporate nonuniformities via coupling of spatial eigenmodes and the occurrence of multiple synaptic receptor types on a single neuron. Further details of the uniform model can be found elsewhere [18,20]. Throughout this work we assume that, in the absence of perturbations, the brain settles into a steady state of activity. The existence and stability of such steady states in our model have been examined in detail in earlier papers [14,15,20]. There it was found that a low-firing rate state exists for physiologically reasonable parameter values; we assume that this state represents the normal state occupied by the brain.

A. Corticothalamic model

Our corticothalamic model incorporates the connectivities shown in Fig. 1, including the thalamic reticular nucleus which inhibits relay nuclei [14–21]. The latter relay external stimuli ϕ_n to the cortex, as well as corticothalamic feedback via projections of ϕ_e to them; their influences are excitatory. The cortex itself is treated as a continuum containing populations of interacting excitatory and inhibitory neurons and is approximated as two dimensional (2D) owing to its relative thinness.

The mean firing rates (i.e., pulse densities) Q_a of excitatory ($a=e$) and inhibitory ($a=i$) neurons are related to the cell-body potentials V_a, relative to resting, by $Q_a(\mathbf{r},t) = S_a[V_a(\mathbf{r},t)]$, where S_a is a smooth sigmoidal function that increases from 0 to $Q_{\max}$ as V_a increases from $-\infty$ to ∞.

The cell-body potential V_a results from the sum of dendritic inputs after they have been filtered in the dendritic tree as they propagate. It approximately [14,18,20] obeys

$$V_a(\mathbf{r},t) = \sum_b V_{ab}(\mathbf{r},t), \tag{1}$$

where V_{ab} is defined by

$$\mathcal{D}_{ab}(\mathbf{r},t) V_{ab}(\mathbf{r},t) = \nu_{ab}(\mathbf{r},t)\phi_b[\mathbf{r},t-\tau_{ab}(\mathbf{r})], \tag{2}$$

$$\mathcal{D}_{ab}(\mathbf{r},t) = \frac{1}{\alpha_{ab}(\mathbf{r})\beta_{ab}(\mathbf{r})}\frac{d^2}{dt^2} + \left[\frac{1}{\alpha_{ab}(\mathbf{r})} + \frac{1}{\beta_{ab}(\mathbf{r})}\right]\frac{d}{dt} + 1, \tag{3}$$

where the right side of Eq. (1) is a sum of contributions from different receptor types b on neurons of type a. The right side of Eq. (2) involves contributions $\phi_{e,i}$ from other cortical neurons, and inputs ϕ_s from thalamic relay nuclei, each delayed by a time $\tau_{ab}(\mathbf{r})$ due to anatomical spatial separation. More generally, each of these could be divided into subtypes corresponding to those incident (afferent) on different receptor populations [e.g., the excitatory glutamate and NMDA (*N*-methyl-*D*-aspartate) types], but we do not make this subdivision here, assuming for simplicity that each neural type corresponds to a single receptor type.

In Eq. (2), $\nu_{ab}(\mathbf{r},t) = N_{ab}(\mathbf{r})s_{ab}(\mathbf{r},t)$, where N_{ab} is the mean number of synapses of type $b=e,i,s$ on neurons of type a and s_{ab} is the strength of the response in neuron a to a unit signal at a synapse of type b. The operator $\mathcal{D}_{ab}$ incorporates synaptodendritic dynamics via the quantities $\beta_{ab}(\mathbf{r})$ and $\alpha_{ab}(\mathbf{r})$, which are the inverse rise and decay times of the cell-body potential produced by an impulse at a dendritic synapse, with $\beta_{ab} \approx 4\alpha_{ab}$ in many cases, owing to dendritic propagation effects [20]. This form of $\mathcal{D}_{ab}$ can be easily generalized to account for more complicated dynamics, and the analytic work in this section does not depend on the precise form (3). Note that we do not include the explicit geometry of the dendrites in our model—only their effect on the temporal characteristics of the signals that pass through them to the cell body.

Each part of the corticothalamic system gives rise to neural pulses, whose values averaged over short scales form a field $\phi_a(\mathbf{r},t)$ ($a=e,i,r,s$ for excitatory, inhibitory, reticular, and relay neurons, respectively) that propagates at $v_a(\mathbf{r}) = 1-10\ \mathrm{m\,s^{-1}}$ ($5-10\ \mathrm{m\,s^{-1}}$ in myelinated fibers and around $1\ \mathrm{m\,s^{-1}}$ in unmyelinated ones). In the regime that is linear in the ϕ_a (which we assume here), linear perturbations approximately obey the damped wave equation [14,18,20]

$$D_a(\mathbf{r},t)\phi_a(\mathbf{r},t) = \rho_a(\mathbf{r},t)V_a(\mathbf{r},t), \tag{4}$$

$$D_a(\mathbf{r},t) = \frac{1}{\gamma_a^2(\mathbf{r})}\frac{\partial^2}{\partial t^2} + \frac{2}{\gamma_a(\mathbf{r})}\frac{\partial}{\partial t} + 1 - r_a^2(\mathbf{r})\nabla^2, \tag{5}$$

where we henceforth use the symbols ϕ_a and V_a to denote linear perturbations to the original versions of these quantities, since there is no possibility of confusion. Here $\gamma_a(\mathbf{r}) = v_a(\mathbf{r})/r_a(\mathbf{r})$, $\rho_a = dS_a(V_a)/dV_a$ is the slope of the sigmoi-

dal function at the assumed steady state value of V_a, and r_a is the characteristic range of axons a. Fourier transformation of Eqs. (1)–(5) in time and elimination of V_a and V_{ab} between these equations yields transfer functions that express the firing rates in terms of the external signal ϕ_n; the poles of these functions yield the linear dispersion characteristics of corticothalamic waves. Note that Eq. (4) does not allow for any variation in ρ_a due to changes in ϕ_a—only variations that result from changes in the parameters of the sigmoidal function are included.

As an aside, if ρ_a are constant in time in Eqs. (1)–(5), they commute with $\mathcal{D}_{ab}$. If all $\mathcal{D}_{ab}$ for given a have a common form $\mathcal{D}_a$ that depends only on a, then

$$\mathcal{D}_a(\mathbf{r},t)D_a(\mathbf{r},t)\,\phi_a(\mathbf{r},t)=\sum_b\, G_{ab}(\mathbf{r},t)\,\phi_b[\mathbf{r},t-\tau_{ab}(\mathbf{r})], \tag{6}$$

with $G_{ab}(\mathbf{r},t)=\rho_a(\mathbf{r})\,\nu_{ab}(\mathbf{r},t)$. Form (6) is not used in the present paper, but is noted for future use.

Fourier transforming Eqs. (1)–(5) in time and eliminating V_a and V_{ab} between these equations yields

$$D_a(\mathbf{r},\omega)\,\phi_a(\mathbf{r},\omega)=\sum_b\, J_{ab}(\mathbf{r},\omega)\,\phi_b(\mathbf{r},\omega), \tag{7}$$

$$J_{ab}(\mathbf{r},\omega)=L_{ab}(\mathbf{r},\omega)G_{ab}(\mathbf{r})e^{i\omega\tau_{ab}(\mathbf{r})}, \tag{8}$$

$$D_a(\mathbf{r},\omega)=(1-i\omega/\gamma_a)^2-r_a^2\nabla^2, \tag{9}$$

where $[L_{ab}(\mathbf{r},\omega)]^{-1}$ is the temporal Fourier transform of $\mathcal{D}_{ab}(\mathbf{r},t)$. Thus for the case of excitatory projections, we have

$$D_e\phi_e=J_{ee}\phi_e+J_{ei}\phi_i+J_{es}\phi_s, \tag{10}$$

where we omit arguments for compactness.

Using the connectivities in Fig. 1 and making the local inhibition approximation, which assumes the short range of inhibitory axons and implies $D_i=D_s=D_r=1$, and random connectivity approximation, in which the numbers of interconnections between neural types are assumed to be proportional to the number of available synapses, we find that $Q_e=Q_i$, $V_e=V_i$, and, hence, $\rho_e=\rho_i$ [18]. This gives

$$\phi_i(\mathbf{r},\omega)=D_e\phi_e(\mathbf{r},\omega), \tag{11}$$

where we also make the assumptions henceforth that all the L_{ab} have a common form L, and that $\tau_{ib}=\tau_{eb}$ for all b. For the specific nuclei, Eq. (7) then becomes

$$\phi_s=J_{se}\phi_e+J_{sr}\phi_r+J_{sn}\phi_n, \tag{12}$$

likewise, for the reticular nucleus we have

$$\phi_r=J_{re}\phi_e+J_{rs}\phi_s. \tag{13}$$

Thus via substitution of Eq. (13) into Eq. (12), we find

$$(1-J_{sr}J_{rs})\,\phi_s=(J_{se}+J_{sr}J_{re})\,\phi_e+J_{sn}\phi_n. \tag{14}$$

Using Eq. (10) then gives an explicit expression for $\phi_s(\mathbf{r},\omega)$ as a function of $\phi_e(\mathbf{r},\omega)$,

$$\phi_s(\mathbf{r},\omega)=[(1-J_{ei})D_e-J_{ee}]\phi_e(\mathbf{r},\omega)/J_{es}. \tag{15}$$

Finally, elimination of ϕ_s and ϕ_r from the above equations results in the transfer function of a stimulus $\phi_n(\mathbf{r},\omega)$ to $\phi_e(\mathbf{r},\omega)$

$$\{(1-J_{sr}J_{rs})[(1-J_{ei})D_e-J_{ee}]-J_{es}(J_{se}+J_{sr}J_{re})\}\phi_e =J_{es}J_{sn}\phi_n, \tag{16}$$

which reproduces our previous results if J_{ab} are spatially uniform [20].

Scalp potentials are primarily generated by excitatory (mainly pyramidal) neurons, because of their greater size and degree of alignment compared to other types [2]. For any given geometry, and in the case of linear perturbations considered here, the scalp potential is proportional to the cortical potential, which is itself proportional to the membrane currents that are present, which are in turn proportional to the firing rate ϕ_e. Hence, apart from a (dimensional) constant of proportionality, the EEG frequency spectrum at $\mathbf{r}$ is thus given by the squared modulus of $\phi_e(\mathbf{r},\omega)$ obtained from Eq. (16). (This neglects volume conduction for reasons discussed in Sec. III D, but this effect can be easily included, as in our previous work [18].) In uniform systems this spectrum shows excellent agreement with observed spectra when physiologically realistic parameters are used in the theory and ϕ_n is assumed to be spatiotemporal white noise [19,20].

B. Coupled mode equations

In the most general case, our transfer function (16) involves multiple position-dependent variables such as the gains G_{ab}, the time delays τ_{ab}, and the filter function L. Here these nonuniformities are treated via the coupling of the spatial eigenmodes.

Equation (16) is of the general form

$$A(\mathbf{r},\omega)\,\phi_e(\mathbf{r},\omega)=B(\mathbf{r},\omega)\,\phi_n(\mathbf{r},\omega). \tag{17}$$

Taking the Fourier transform in space and assuming periodic boundary conditions on a rectangular cortex of size $l_x\times l_y$ (or of length l_x in 1D), this expression becomes a discrete convolution:

$$\sum_{\mathbf{K}}\, A(\mathbf{k}-\mathbf{K},\omega)\,\phi_e(\mathbf{K},\omega)=\sum_{\mathbf{K}}\, B(\mathbf{k}-\mathbf{K},\omega)\,\phi_n(\mathbf{K},\omega). \tag{18}$$

Here $\mathbf{k}$ and $\mathbf{K}$ range over the values $\mathbf{k}_{mj}$, $\mathbf{K}_{mj}=(2\pi m/l_x, 2\pi j/l_y)$ in 2D, where i and j are integers (and over the values $2\pi m/l_x$ in 1D). The imposition of boundary conditions has previously been shown to affect spectra at very low frequencies and near the alpha peak; however, it does not, in itself, appear to lead alpha splitting consistent with observations [19], and thus the precise boundary conditions chosen are not expected to be critical. (Physically, this results from the strong spatial damping of waves, except at

resonances in the spectrum: strongly damped waves are not sensitive to boundary conditions, since their characteristic spatial scale is not sufficent to "sense" them [19].) Analogous expressions can readily be obtained for a spherical cortex, for example, involving a spherical harmonic expansion of modes with Clebsch-Gordan coefficients describing the mode couplings.

Equation (18) shows the essential feature of mode coupling: the value of ϕ_e at a particular wave number is thus a function of the values at other wave numbers. This is unlike the case of waves in a uniform medium, where each wave number is independent of all the others. This coupling is induced because modulation of the properties of the medium at a wave number $\mathbf{q}$ induces a response at $\mathbf{k}+\mathbf{q}$ in a wave with initial wave number $\mathbf{k}$. Examples of this effect in other physical systems are mentioned in Sec. III B.

In order to solve Eq. (18) for $\phi_e(\mathbf{k},\omega)$, the first step is to truncate the set of modes to $|m|,|j| \leqslant M_{\max}$ for some $M_{\max}$. We then write $\phi_e(\mathbf{k},\omega)$ and $\phi_n(\mathbf{k},\omega)$ as column vectors (one row per mode), Φ_e and Φ_n, using an appropriate (but arbitrary in general) ordering of modes. In 1D no special labeling is necessary, and the mode and row numbers can be set equal. A useful 2D relabeling is

$$\mu(m,j) = m + (2M_{\max}+1)j, \tag{19}$$

where m and j are the 2D subscripts of $\phi_e(\mathbf{k}_{mj},\omega)$, and $\mu(m,j)$ is the corresponding matrix index. This form is particularly useful because of the symmetry between the positive and negative terms, with $\mu(-m,-j) = -\mu(m,j)$.

Equation (18) can be written as a matrix equation $\mathbf{A}\Phi_e = \mathbf{B}\Phi_n$ where, in 1D, $\mathbf{A}$ and $\mathbf{B}$ are $(2M_{\max}+1)\times(2M_{\max}+1)$ matrices, and Φ_e and Φ_n are column matrices with $(2M_{\max}+1)$ terms. [In 2D, $\mathbf{A}$ and $\mathbf{B}$ are $(2M_{\max}+1)^2\times(2M_{\max}+1)^2$ matrices, and Φ_e and Φ_n are column matrices with $(2M_{\max}+1)^2$ terms.] Consequently,

$$\Phi_e = \mathbf{A}^{-1}\mathbf{B}\Phi_n, \tag{20}$$

$$= \mathbf{M}\Phi_n, \tag{21}$$

which defines the matrix $\mathbf{M}$. Thus $\phi_e(\mathbf{K}_{mj},\omega)$ can be calculated by matrix inversion. The spatially averaged power spectrum $P(\omega)$ can then be obtained via matrix multiplication, with

$$P(\omega) = \Phi_e^{\dagger}(\omega)\Phi_e(\omega), \tag{22}$$

$$= \sum_{\mathbf{K}} |\phi_e(\mathbf{K},\omega)|^2, \tag{23}$$

where $\Phi_e^{\dagger}$ is the Hermitian conjugate of Φ_e.

The power spectrum at a given $\mathbf{r}$ is then

$$P(\mathbf{r},\omega) = |\phi_e(\mathbf{r},\omega)|^2, \tag{24}$$

$$\phi_e(\mathbf{r},\omega) = \sum_{\mathbf{K}} \phi_e(\mathbf{K},\omega) e^{i\mathbf{K}\cdot\mathbf{r}}. \tag{25}$$

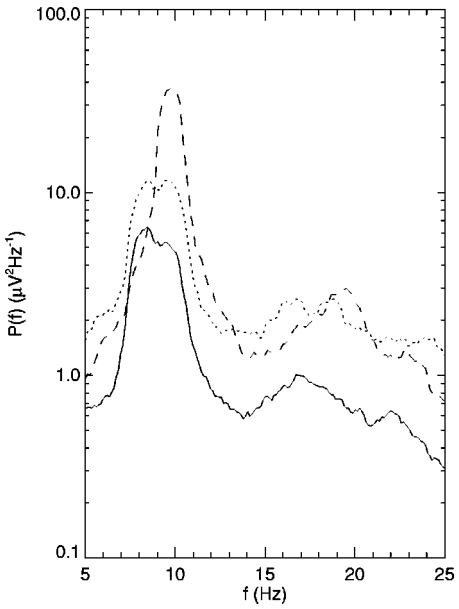

FIG. 2. The Fp_1 (left frontal pole, solid curve), Cz (central midline, dotted curve), and O_2 (right occipital, dashed curve) single-electrode spectra of a typical split-alpha subject, taken when eyes are closed, and subject is relaxed. The alpha peak near 8 Hz dominates frontally, while that near 10 Hz dominates at the back of the head. At the Cz electrode, a double peak is seen, with both frequencies represented.

When averaged over the random phases of spatially white noise of root-mean-square amplitude $|\phi_n(\omega)|$, this yields

$$P(\mathbf{r},\omega) = |\phi_n(\omega)|^2 \sum_{\mu,\nu} \exp[i(\mathbf{k}_\mu - \mathbf{k}_\nu)\cdot\mathbf{r}](\mathbf{M}\mathbf{M}^{\dagger})_{\mu\nu}, \tag{26}$$

where μ and ν label matrix elements as in Eq. (19). By averaging Eq. (26) over position, Eq. (22) can thus be written in the equivalent form, for spatially white noise,

$$P(\omega) = |\phi_n(\omega)|^2 \,\mathrm{Tr}(\mathbf{M}\mathbf{M}^{\dagger}). \tag{27}$$

If the noise is also temporally white, $\phi_n(\omega)$ is independent of ω.

III. SPLIT-ALPHA PEAKS

It has been suggested that nonuniformities in corticothalamic time delays may underlie the observed splitting of alpha peaks in a few percent of subjects [19]. Certainly, the alpha frequency is most sensitive to t_0 among the parameters of our model [18]. Such a split-alpha peak is illustrated in Fig. 2, using data from an existing database that was collected with appropriate ethical clearances and informed consent [22]. Data were recorded in the relaxed eyes-closed state at a 250 Hz sampling rate relative to a linked-ears reference using a low-pass filter with -6 dB point at 50 Hz, then processed to remove ocular artifacts [22]. Spectra were calculated for 15 successive 8-s segments of data to improve the signal-to-noise ratio, then averaged to obtain the curves in Fig. 2 for three electrodes spanning a semicircle on the head:

TABLE I. Nominal values of model parameters for an eyes-closed state with alpha rhythm, close to those used in Ref. [20]. The mean excitatory axonal range is r_e, l_x approximates the circumference of the cortex, taking into account its folding (scalp distances are approximately 2/3 as large as cortical ones), γ_e is the cortical damping rate, α and β are dendritic time constants, T_0 is the mean roundtrip delay for signals traveling from the cortex to the thalamus and back, and the quantities G_{ab} are the gains for signals from neurons of type b incident on neurons of type a. Only those gains or products of gains that occur in Sec. III A are listed.

Quantity	Nominal	Unit
r_e	0.08	m
l_x	0.8	m
γ_e	120	s^{-1}
$\alpha=\beta/4$	60	s^{-1}
T_0	80	ms
G_{ee}	4.5	
G_{ei}	−5.5	
G_{es}	4.0	
$G_{es}G_{sr}G_{re}$	−4.0	
$G_{es}G_{se}$	9.0	
$G_{sr}G_{rs}$	−1.5	

Fp_1 (frontal pole, located slightly left of center at the crown of the forehead), Cz (central, located on the midline at the top of the head), and O_2 (occipital, located slightly right of center at the back of the head). The subject used was a normal female of age 62 years with a split-alpha spectrum. The short duration of the measurements overall (just 2 min) allows nonstationarity to be neglected to a good approximation. In particular, we find no evidence for nonstationarity in the alpha frequency, even over longer time periods.

In this section we illustrate and discuss the general results of the preceding section in the context of split-alpha spectra, with $\tau_{es}(\mathbf{r})=\tau_{se}(\mathbf{r})=\tau_{re}(\mathbf{r})=t_0(\mathbf{r})/2$ and the other τ_{ab} all zero, which generalizes our previous work to include nonuniformities. For simplicity, we assume that G_{ab}, L, γ_a, and r_a are uniform in space, assumptions that can be straightforwardly relaxed if required. The derivation is carried out for the 2D case, but only the 1D case is explored numerically since previous work showed that 1D and 2D spectra are very similar [19] and the results here are only intended to be illustrative, with a full statistical study to be published later in the clinical literature.

Henceforth, except where otherwise stated, we use model parameters very similar to those employed in our previous studies [20], as listed in Table I. This approach emphasizes the consistency of the present work with previous results. Future work will explore optimal fitting of all parameters to EEG data using the full 2D numerics.

A. Nonuniform time delay model

We use the above general derivation to calculate the spectra for a nonuniform corticothalamic time delay $t_0(\mathbf{r})$, by setting

$$t_0(\mathbf{r})=T_0+\tau(\mathbf{r}), \tag{28}$$

where T_0 is the average of $t_0(\mathbf{r})$ over position. After division by $(1-H_{sr}H_{rs})(1-H_{ei})$, Eqs. (8) and (16) yield

$$\left[D_e-\frac{H_{ee}}{1-H_{ei}}-\frac{H_{es}(H_{se}+H_{sr}H_{re})e^{i\omega t_0(\mathbf{r})}}{(1-H_{sr}H_{rs})(1-H_{ei})}\right]\phi_e(\mathbf{r},\omega)$$
$$=\frac{H_{es}H_{sn}e^{i\omega t_0(\mathbf{r})/2}}{(1-H_{sr}H_{rs})(1-H_{ei})}\phi_n(\mathbf{r},\omega), \tag{29}$$

$$H_{ab}=G_{ab}L(\omega). \tag{30}$$

If we then expand the exponentials to first order in $\tau(\mathbf{r})$ to give $\exp[i\omega\tau(\mathbf{r})/2]\approx 1+i\omega\tau(\mathbf{r})/2$, and then Fourier transform in $\mathbf{r}$, we obtain

$$\phi_e(\mathbf{k},\omega)-C(\mathbf{k},\omega)\sum_{\mathbf{K}}\tau(\mathbf{k}-\mathbf{K})\phi_e(\mathbf{K},\omega)$$
$$=\sum_{\mathbf{K}}N(\mathbf{k}-\mathbf{K},\omega)\phi_n(\mathbf{K},\omega), \tag{31}$$

$$C(\mathbf{k},\omega)=\frac{i\omega e^{i\omega T_0}H_{es}(H_{se}+H_{sr}H_{re})}{(1-H_{ei})(1-H_{sr}H_{rs})(k^2r_e^2+q^2r_e^2)}, \tag{32}$$

$$N(\mathbf{k}-\mathbf{K},\omega)=\frac{H_{es}H_{sn}e^{i\omega T_0/2}}{(1-H_{ei})(1-H_{sr}H_{rs})(k^2r_e^2+q^2r_e^2)}$$
$$\times[\delta(\mathbf{k}-\mathbf{K})+i\omega\tau(\mathbf{k}-\mathbf{K})/2], \tag{33}$$

$$q^2(\omega)r_e^2=\left(1-\frac{i\omega}{\gamma_e}\right)^2-\frac{1}{1-H_{ei}}$$
$$\times\left[H_{ee}+\frac{H_{es}(H_{se}+H_{sr}H_{re})e^{i\omega T_0}}{1-H_{sr}H_{rs}}\right]. \tag{34}$$

The sums over $\mathbf{K}$ in Eq. (31) appear because the Fourier transforms of the products $\tau(\mathbf{r})\phi_e(\mathbf{r},\omega)$ and $\tau(\mathbf{r})\phi_n(\mathbf{r},\omega)$ yield convolutions of this form. Equation (29) is easily written in the form (18), with

$$A(\mathbf{k},\mathbf{K},\omega)=\delta(\mathbf{k}-\mathbf{K})-C(\mathbf{k},\omega)\tau(\mathbf{k}-\mathbf{K}), \tag{35}$$

$$B(\mathbf{k},\mathbf{K},\omega)=N(\mathbf{k}-\mathbf{K},\omega), \tag{36}$$

and can thus be reduced to matrix form, as in the general case. In terms of matrix elements, Eqs. (29), (35), and (36) can be written as

$$A_{\mu\nu}=\delta_{\mu\nu}-C_\mu\tau_{\mu-\nu}, \tag{37}$$

$$B_{\mu\nu}=N_{\mu\nu}. \tag{38}$$

To illustrate the effects of spatial variation of t_0 explicitly in a simple 1D case, we take

$$t_0(x)=T_0+\tau_1e^{ik_1x}+\tau_{-1}e^{-ik_1x}, \tag{39}$$

where $\tau_1=\tau_{-1}^*$ since $t_0(x)$ is real and $k_1=2\pi/l_x$. For simplicity, our simulations use real values with $\tau_1=\tau_{-1}$, since use of complex values merely shifts $t_0(x)$ along the x axis and we have assumed periodic boundary conditions. In this case, $t_0(x)=T_0+2\tau_1\cos(k_1x)$ and the range of $t_0(x)$ is $|t_0(x)-T_0|\leqslant 2|\tau_1|$. Hence, the requirement that $|\omega\tau|\lesssim 2$ implies $|\tau_1|\lesssim 8$ ms at the $\sim$10-Hz alpha peak and $|\tau_1|\lesssim 4$ ms at the $\sim$20-Hz beta peak for our approximations to be valid. This restriction could be relaxed by Fourier transforming A and B numerically for a chosen form of spatial variation, in which case no such approximation would be made.

B. Spatially averaged spectra

Examples of theoretical spectra are shown in Fig. 3 for the nominal parameters in Table I. For later comparison of our results with scalp EEG data, we let $x=0$ correspond to the front of the cortex, since preliminary inspection of the data shows a tendency for lower alpha frequencies in this region. We also let $x=l_x/2$ correspond to the most posterior region of the cortex, where l_x is the linear size of the cortex (about 1.5 times the circumference of the head, owing to cortical folding [2]). Hence, we assume that $t_0(x)$ is maximal at the front of the head and minimal at the back if τ_1 is positive. Actual variations of $t_0(x)$ may be more complicated, but form (39) is sufficient to illustrate the principles involved. The use of the circumference of the cortex as the value of l_x is the most appropriate choice for comparison with a 1D calculation. In any case, the value of l_x does not strongly affect spectra unless it is considerably smaller [19].

When $\tau_{\pm 1}=0$ ms (no nonuniformity and hence no mode coupling), seen in Fig. 3(a), the spectrum is seen to have alpha and beta peaks at around 9.5 Hz and 17.8 Hz, respectively. There is a small-amplitude splitting in the alpha peak, which is due to the discrete mode structure imposed by the cortex [19], as seen from the relative contributions of the 0 and ± 1 modes, which have similar peak powers, while the ± 2 modes (not shown) are comparable to these only above about 15 Hz. Investigation shows that this splitting is only observable for relatively sharp alpha peaks [19], such that the separation of the modes is greater than their widths; it disappears if $G_{es}G_{se}$ is reduced by less than 10%, for example.

At $\tau_{\pm 1}=3$ ms in Fig. 3(b), a splitting of greater amplitude and frequency separation is seen. The spectra of individual spatial eigenmodes show that this is due to the appearance of structure in each of the $0,\pm 1$ modes. This results from their coupling via the spatial variation of τ: the 0 mode drives the ± 1 modes most strongly at its peak frequency, and vice versa.

At $\tau_{\pm 1}=6$ ms, Fig. 3(c) shows greater peak separation and more substructure in each mode. As $\tau_{\pm 1}$ continues to increase, these trends persist, although no additional peaks are seen for $\tau_1\leqslant 7$ ms. There is also a gradual downshift of the beta peak to around 16.9 Hz at $\tau_1=6$ ms, but this peak is sufficiently broad that substructures and frequency shifts in individual modes do not produce multiple peaks in the overall spectrum in this case.

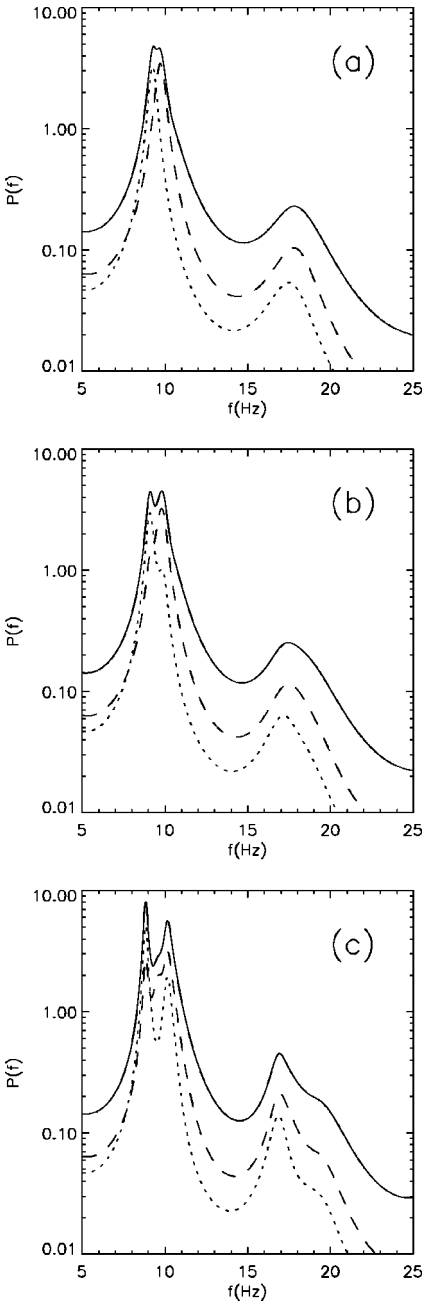

FIG. 3. (a) Coupled power spectra (solid curves, arbitrary units) for various values of $\tau_{\pm 1}$, with other parameters as in Table I. Also shown are the 0 mode power (dotted curves) and the sum of the ± 1 mode powers (dashed curves). (a) $\tau_{\pm 1}=0$ ms, (b) $\tau_{\pm 1}=3$ ms, (c) $\tau_{\pm 1}=6$ ms.

The mechanism of split-alpha generation inferred in the previous paragraphs involves coupling of weakly damped spatial modes via nonuniformities in $t_0(\mathbf{r})$. Unlike previous suggestions [2,9], these modes are not purely cortical, and are weakly damped only because of the existence of cortico-thalamic loops with appropriate gains [18–20]. In addition, the nature of the coupling is such that it produces multiple frequency peaks in each mode's spectrum, rather than each mode having a separate peak, as assumed in proposed mechanisms based on purely cortical modes without mode-

mode coupling. We investigate coupling further shortly.

Waves at a given location are generated most strongly with an alpha period approximately related to the local corticothalamic loop delay in the same manner as in the uniform case, giving [18,20]

$$T_\alpha(x)=[f_\alpha(x)]^{-1}\approx t_0(x)+1/\alpha+1/\beta, \tag{40}$$

where $\Delta t=1/\alpha+1/\beta$ is the part of the corticothalamic loop delay that is due to dendritic propagation. Maximal contributions to the spatially averaged spectrum arise from turning points of $t_0(x)$, where $T_\alpha(x)$ is stationary. For our choice (39), this gives extremal periods deviating by $\pm 2\tau_1$ from the uniform case. Periods corresponding to observed spectral peaks (as opposed to peaks of the local contribution alone) must lie between these bounds, even when electrodes are placed at extremums of $\tau(\mathbf{r})$, since the spectrum measured at any point contains contributions from other locations, via cortical propagation.

It is easily verified that alpha splitting in our model is due to coupling of modes via the inhomogeneity, not to shifts in the individual mode frequencies themselves. One computes the overlap integral (in Dirac notation) of the inhomogeneity, taken between unperturbed real modes of the form

$$|m_+\rangle=(2/l_x)^{1/2}\cos(k_m x), \tag{41}$$

$$|m_-\rangle=(2/l_x)^{1/2}\sin(k_m x), \tag{42}$$

for $m>0$ without loss of generality. This gives the expectation value (in effect, a weighted average of all the values encountered by the modes in question) of the shift in period to be

$$\langle m_+|\tau|n_+\rangle=\frac{2}{l_x}\int_0^{l_x}\cos(k_m x)\,\tau(x)\cos(k_n x)\,dx, \tag{43}$$

$$=\tau_1[\delta_{m,n+1}+\delta_{m,n-1}], \tag{44}$$

$$=-\langle m_-|\tau|n_-\rangle, \tag{45}$$

$$\langle m_+|\tau|n_-\rangle=\langle m_-|\tau|n_+\rangle=0, \tag{46}$$

for form (39), with $\tau(x)=2\tau_1\cos(k_1 x)$. From these results we see that the modes undergo no first-order shift in period, since $\langle m_\pm|\tau|m_\pm\rangle=0$ for all combinations of signs. Mode coupling produces additional peaks shifted by $\pm\tau_1$ and will have large contributions to the total spectrum for modes which are themselves strong and which couple to other strong modes—i.e., for the 0, ± 1, and (possibly) ± 2 modes. These new peaks can themselves couple via the inhomogeneity to produce further peaks. More complicated variations than Eq. (39) will have more Fourier coefficients and, hence, will couple larger ranges of modes. Incidentally, the coupling in Eq. (43) is analogous in optics to scattering of an incoming wave $|n\rangle$ off a grating formed by τ into an outgoing wave $\langle m|$ with a different wave vector. Alternatively, it is analogous in quantum physics (whence the notation is derived) to coalescence or decay of one wave quantum into another, with involvement of a third quantum, corresponding to a potential whose role is played by τ.

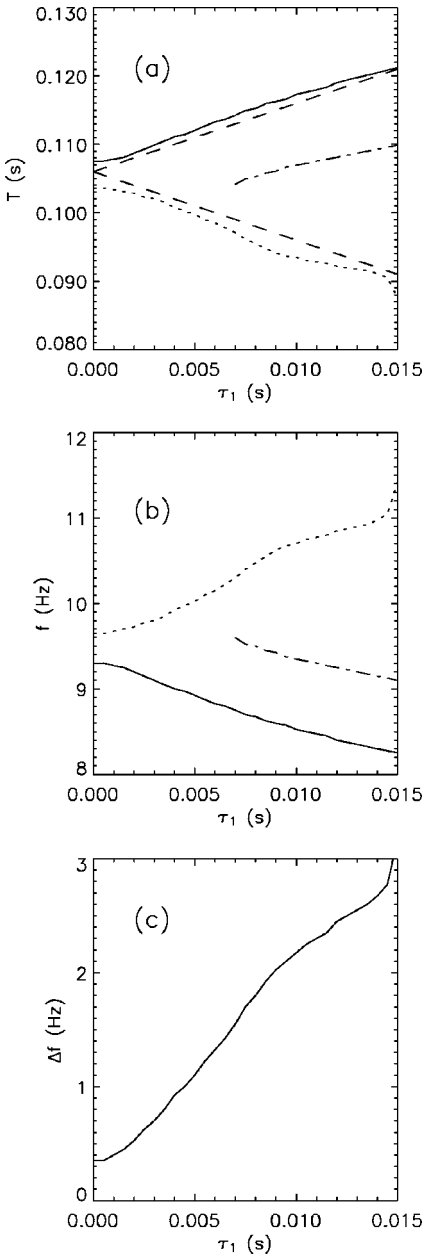

FIG. 4. Parameters of alpha peaks in Fig. 3, vs τ_1. The higher frequency peak is shown as dashed lines and the lower frequency one as solid. Where a third peak exists, it is shown in triple-dot-dashed style. (a) Periods, with dotted curves showing offsets of $\pm\tau_1$ from the mean unperturbed value for comparison; (b) frequencies; (c) overall frequency splitting Δf.

Figure 4 shows the periods, frequencies, and frequency separation $\Delta f=f_+-f_-$ of the alpha peaks in Fig. 3 as functions of τ_1, where f_+ is the highest alpha peak frequency and f_- is the lowest. Figure 4(a) shows the small splitting at $\tau_1=0$, and confirms the approximately linear dependence on τ_1 for larger values. The upper and lower periods in Fig. 4(a) are displaced from the uniform value by $\pm\tau_1$, in good agreement with Eqs. (43)–(45). Figures 4(b) and 4(c) show that a typical observed splitting of 1 Hz (in those subjects with

split-alpha peaks) corresponds to $\tau_1 \approx 5$ ms. The third peak appearing for $\tau_1 \gtrsim 7$ ms in Fig. 4 results from coupling of each of the two outer peaks with the inhomogeneity to produce a peak near the unperturbed frequency. This peak is seen to drift slightly with τ_1, because it distorted as a result of being superposed on the contributions of the other peaks, which are not of equal intensity.

C. Locally measured spectra

We explore the spatial dependence of power spectra in Fig. 5, which shows spectra obtained at various locations using Eq. (27) with white noise inputs. The parameters in Table I are used, with $\tau_{\pm 1} = 6$ s, which corresponds to an alpha splitting in the mean spectrum of around 1.2 Hz. At small x (frontally here), Fig. 5(a) shows that the lower side of the alpha peak is enhanced relative to the mean, whereas the enhancement moves progressively to the high frequency side at larger x (central and posterior locations), as shown in Figs. 5(b) and 5(c). These trends are in accord with Eq. (40). The beta peak moves to higher frequency and becomes broader and less prominent as x increases, which explains why the mean spectrum is skewed toward lower frequencies.

Figure 6 shows $P(x,\omega)$ as a function of position and frequency. This demonstrates more clearly the close correlation between $T_\alpha(x)$, given by Eq. (40), and the peak in locally measured power. However, Fig. 6 also shows that this correlation is not perfect, owing to the cortical propagation of power between locations. This is seen most clearly in the projection of the strong peak at $x = 0$ at fixed frequency as far as $x \approx 0.20$ m, even while contours at other frequencies roughly follow the variation in $t_0(x)$.

To illustrate further the way in which $P(x,\omega)$ reflects local variations in $t_0(x)$, we show this quantity in Fig. 7 for

$$t_0(x) = T_0 + \tau_1 \exp[-x^2/(\Delta x)^2], \tag{47}$$

with $\tau_1 = 20$ ms and $\Delta x = 0.04$ m, and where T_0 is a base level, rather than the average value used previously. At the peak, the intense signal spreads well beyond its local point of generation, but the effects of the inhomogeneity on the spectrum are better localized to its vicinity at other (more heavily damped) frequencies. Hence, even spatially small sources of alpha can potentially be localized by spectral measurements, so long as these accurately capture frequencies away from the peaks.

D. Illustrative comparison with data

The variations in the structure of the alpha peak inferred above are in good qualitative accord with those seen in Fig. 2, whose alpha frequencies imply $\tau_1 \approx 8$ ms for this subject, since

$$\tau_1 \approx \frac{1}{2f_-} - \frac{1}{2f_+}. \tag{48}$$

Hence, Figs. 3(c) and 5 can be compared with Fig. 2, but the relative normalizations of the curves from different electrodes cannot be compared between theory and data here, because of the unknown effects of variable skull thickness and variable white noise amplitude, in particular, on the relative strength of the scalp spectra at various locations. The related effect of k-dependent filtering by volume conduction, which removes short-scale features in the signals, can be ignored at the alpha peak because it is significant only for $k \gtrsim 15$ m^{-1} [18,23], whereas $k_{\pm 1} \approx 8$ m^{-1}. The beta peak has similar spectral trends, but these do not result in splitting of the theoretical spectrum, whereas the observed beta peak shows some sign of splitting, with subpeaks around 17 Hz and 18.5 Hz. We note, however, that the theoretical analysis

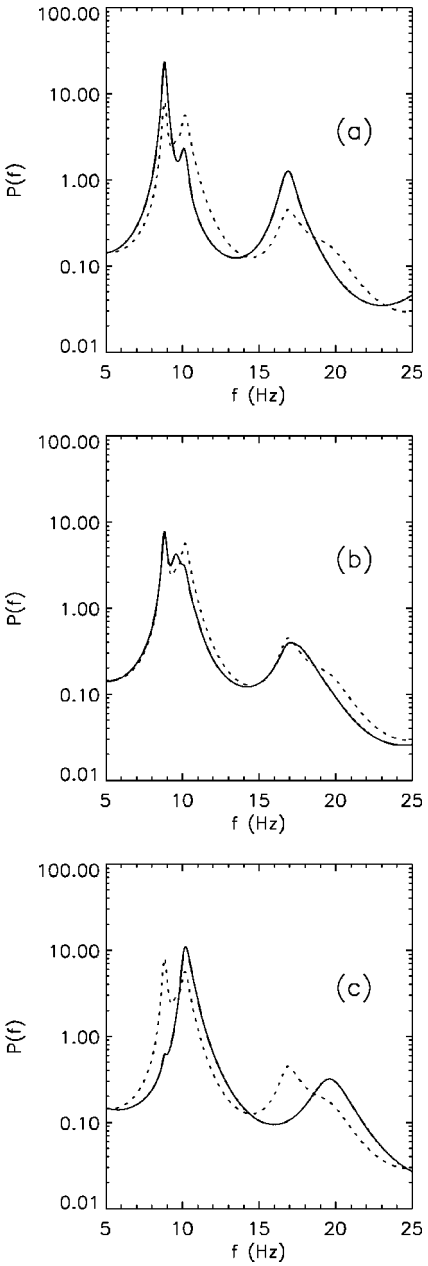

FIG. 5. Locally measured power spectra (solid curves, arbitrary units) for $\tau_1 = 6$ ms, and other parameters as in Table I, for various values of x. The mean spectrum is overplotted for comparison (dotted curves). (a) $x = 0$, $t_0(x) = 92$ ms. (b) $x = 0.16$ m, $t_0(x) = 84.5$ ms. (c) $x = 0.4$ m, $t_0(x) = 68$ ms.

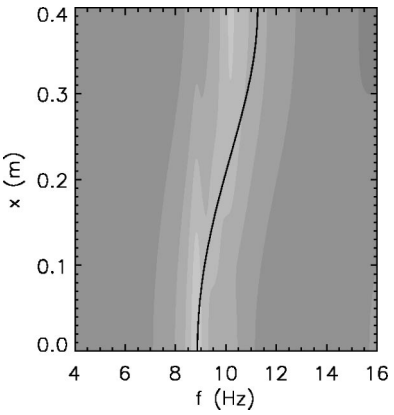

FIG. 6. Locally measured power $P(x,f)$ (arbitrary units) vs frequency and position for a cosine variation of $t_0(x)$, as in Eq. (39), with dark shades indicating low levels, and gray levels logarithmically spaced, half a decade apart. $T_\alpha(x)$ (dashed curve), estimated using Eq. (40), is overplotted for comparison. The parameters are those of Table I, with $\tau_1=6$ ms in the form (39) of $t_0(x)$.

is at or beyond its limit of validity in the beta range, so we do not pursue this comparison further.

The theoretical behavior is robust within the parameter ranges that correspond to strong alpha peaks: parameter changes that enhance the peak (i.e., make it less damped) favor alpha splitting by narrowing the individual mode widths, while splitting in the absence of inhomogeneity is favored by decreasing l_x, which increases the natural frequency separation between the 0 and ± 1 modes.

Visual examination of 100 sets of spectra obtained from normal subjects by the same means as Fig. 2 reveals approximately 80 with clear alpha peaks under the experimental conditions used, including eight with unequivocal split-alpha peaks. However, roughly another third of the 80 showed a readily discerned front-to-back trend in the alpha frequency, in most cases increasing toward the back. These features are consistent with the literature on incidence and frequency of alpha peaks [1], although we are not aware of any published estimate of the incidence of split alpha. Detailed analysis of these data will be published in the clinical literature, but we conclude that at least 10% of subjects with alpha have split alpha discernable at the Cz electrode and, hence, $\tau_1 \gtrsim 5$ ms. Roughly another 25% of subjects with alpha have a noticeable increase in alpha frequency toward the posterior, implying τ_1 of a few ms, while a few percent have a trend in the opposite direction, implying a negative τ_1 of a few ms. The remaining (roughly half) of the alpha subjects are inferfed to have $|\tau_1| \lesssim 2-3$ ms, since no clear frequency trend was discerned on visual inspection. These preliminary results are thus consistent with split alpha subjects corresponding to the tail of a statistical distribution of τ_1 values, which parametrize corticothalamic inhomogeneity with a positive mean of around 1 ms and a standard deviation of a couple of ms.

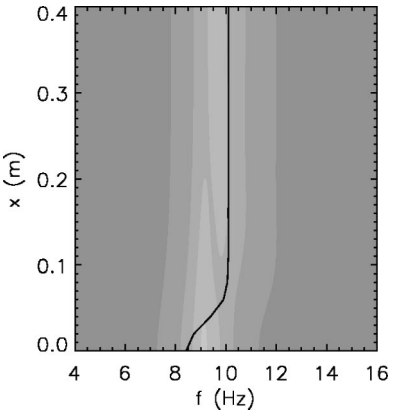

FIG. 7. Locally measured power $P(x,f)$ (arbitrary units) vs frequency and position for a Gaussian variation of $t_0(x)$, as in Eq. (47), with dark shades indicating low levels, and gray levels logarithmically spaced, half a decade apart. The local value of $T_\alpha(x)$ (dashed curve), estimated using Eq. (46), is overplotted for comparison. The parameters are those of Table I, with $\tau_1=20$ ms in form (47) of $t_0(x)$.

IV. SUMMARY AND DISCUSSION

We have included parameter nonuniformities in our previous continuum model of the generation of EEG signals, via their coupling of spatial eigenmodes. This approach yields a matrix equation for the coupled mode amplitudes, which can be inverted to yield the amplitudes, and local and mean spectra. To illustrate the method, we have used it to investigate the effect of spatially nonuniform corticothalamic time delays on the splitting of the alpha peak that is seen in a small percentage of the normal population.

Theoretically, we find that modal structure (involving the 0 and ± 1 modes in the 1D case) can produce a small splitting in the alpha peak, even in the absence of nonuniformity. This is most likely to occur for sharp peaks and if the cortex is small. For $\tau_1 \gtrsim 5$ ms, nonuniformity generally dominates, with the peak separation being linearly dependent on τ_1. The frequency of the local spectral peak trends in the same direction as the local corticothalamic time delay, although waves generated at one location contribute at others, due to cortical propagation, especially if generated at sharp (hence, weakly damped) spectral peaks. This propagation effect leads to intermediate values of periods for measured peaks, which contain contributions from multiple locations. Split-alpha peaks should thus be most readily observed at central electrodes, where contributions are received from both front and back of the head where alpha frequencies are extremal. Variations in the alpha frequency can also probe quite localized variations in corticothalamic inhomogeneity, as shown by our results.

The mechanism of alpha splitting in our theory is via mode coupling induced by spatial nonuniformities. This is predicted to be strongest for the lowest-order modes and leads to each mode developing additional peaks with periods displaced by $\pm \tau_1$ relative to their unperturbed values, which are unchanged to first order. This contrasts with alternative explanations involving (i) *ad hoc* pacemakers, or (ii) splitting of the degeneracy of modes, which would leave the 0 mode unsplit and presumes a single peak for each mode [2,9,19]. The mechanism we propose does rely on weakly damped eigenmodes, as in (ii), but these are weakly damped in our model only as a result of corticothalamic feedback, and each develops multiple peaks as a result of mode coupling.

Our calculations semiquantitatively match the trends seen in EEG data for physiologically realistic input parameters, with $|\tau_1| \gtrsim 5$ ms for distinct split-alpha peaks to be seen. Based on visual inspection of trends in spectra without distinct split alpha, we suggest that split-alpha subjects form the tail of the distribution of τ_1 values in normal subjects, rather than a separate population. Most subjects are inferred to have $|\tau_1| \lesssim 2-3$ ms. A detailed analysis of these data will be published in the clinical literature.

In addition to the above specific findings, the present work provides a motivation for better direct physiological measurements of corticothalamic loop delays to provide more stringent tests of its predictions. Another area for future work is the application of the general analysis in Sec. II to other nonuniformities in the cortex.

ACKNOWLEDGMENTS

We thank S. C. O'Connor for helpful comments on the manuscript and numerics. This work was supported by a University of Sydney Sesqui grant and the Australian Research Council.

[1] E. Niedermeyer and F.H. Lopes da Silva, *Electroencephalography: Basic Principles, Clinical Applications, and Related Fields*, 4th ed. (Williams and Wilkins, Baltimore, 1999).
[2] P.L. Nunez, *Neocortical Dynamics and Human EEG Rhythms* (Oxford University Press, Oxford, 1995).
[3] A.M.L. Coenen, Neurosci. Biobehav. Rev. **19**, 447 (1995).
[4] H.R. Wilson and J.D. Cowan, Kybernetik **13**, 55 (1973).
[5] F.H. Lopes da Silva, A. Hoeks, H. Smits, and L.H. Zetterberg, Kybernetik **15**, 27 (1974).
[6] P.L. Nunez, IEEE Trans. Biomed. Eng. **21**, 473 (1974).
[7] W.J. Freeman, *Mass Action in the Nervous System* (Academic, New York, 1975).
[8] F.H. Lopes da Silva, J.E. Vos, J. Mooibroek, and A. van Rotterdam, Electroencephalogr. Clin. Neurophysiol. **50**, 449 (1980).
[9] P.L. Nunez, *Electric Fields of the Brain* (Oxford University Press, Oxford, 1981).
[10] M. Steriade, P. Gloor, R.R. Llinás, F.H. Lopes da Silva, and M.-M. Mesulam, Electroencephalogr. Clin. Neurophysiol. **76**, 481 (1990).
[11] W.J. Freeman, Int. J. Bifurcation Chaos **2**, 451 (1992).
[12] J.J. Wright and D.T.J. Liley, Behav. Brain Sci. **19**, 285 (1996).
[13] V.K. Jirsa and H. Haken, Phys. Rev. Lett. **77**, 960 (1996).
[14] P.A. Robinson, C.J. Rennie, and J.J. Wright, Phys. Rev. E **56**, 826 (1997).
[15] P.A. Robinson, C.J. Rennie, J.J. Wright, and P.D. Bourke, Phys. Rev. E **58**, 3557 (1998).
[16] C.J. Rennie, P.A. Robinson, and J.J. Wright, Phys. Rev. E **59**, 3320 (1999).
[17] C.J. Rennie, J.J. Wright, and P.A. Robinson, J. Theor. Biol. **205**, 17 (2000).
[18] P.A. Robinson, C.J. Rennie, J.J. Wright, H. Bahramali, E. Gordon, and D.L. Rowe, Phys. Rev. E **63**, 021903 (2001).
[19] P.A. Robinson, P.N. Loxley, S.C. O'Connor, and C.J. Rennie, Phys. Rev. E **63**, 041909 (2001).
[20] P.A. Robinson, C.J. Rennie, and D.L. Rowe, Phys. Rev. E **65**, 041924 (2002).
[21] C.J. Rennie, P.A. Robinson, and J.J. Wright, Biol. Cybern. **86**, 457 (2002).
[22] A.R. Haig, E. Gordon, G. Rogers, and J. Anderson, Electroencephalogr. Clin. Neurophysiol. **94**, 288 (1995).
[23] S.C. O'Connor, P.A. Robinson, and A.K.I. Chiang, Phys. Rev. E **66**, 061905 (2002).